Support Information

A Multifunctional Paper-based Supercapacitor with Excellent Temperature Adaptability, Plasticity, Super-tensile, Self-healing and High Thermoelectric Effect

Chuanyin Xiong[1*], Qi Yang[1], Weihua Dang[1], Qiusheng Zhou[1], Xue Jiang[1], Xuhui Sun[2], Zequn Wang[2], Meng An[2*], Yonghao Ni[3]

[1]College of Bioresources Chemical & Materials Engineering, Shaanxi University of Science and Technology, Xi'an 710021, China

[2]College of Mechanical and Electrical Engineering, Shaanxi University of Science & Technology, Xi'an 710021, China

[3]Department of Chemical and biomedical Engineering, University of Maine, Orono, Maine, 04469, USA

Email: xiongchuanyin@126.com; xiongchuanyin@sust.edu.cn; anmeng@sust.edu.cn

1. Experimental details

1.1 Materials

PVA and $ZnCl_2$ are supplied by Damao Reagent Co., Ltd., China. All the reagents are of analytical grade and used without purification. Ordinary household rolls are purchased from supermarkets.

1.2 Synthesis of carbonized activated paper carbon (APC)

Ordinary household rolls were cut to the required thickness and then stabilized at 250 ℃ at 3 ℃ min^{-1} for 4 h, followed by carbonization in argon at a heating rate of 5 ℃ min^{-1} at 800 ℃ for 3 h.

1.3 Synthesis of APC-PVA@$ZnCl_2$ composite

The polyvinyl alcohol (50 g) was completely dissolved in 250 mL deionized water at 85 ℃, and 15 g zinc chloride solution was added after the polyvinyl alcohol was completely dissolved, and then stirred evenly at 85 ℃. After the solution thickened, the composite electrode material APC-PVA@$ZnCl_2$ was obtained after cooling and standing, and then rotated on the carbonized paper of the upper sequence.

1.4 Electrochemical characterization

The electrochemical properties of APC-PVA@$ZnCl_2$ integrated supercapacitors were studied by CHI760E Electrochemical Workstation (Chenhua, Shanghai). Since the material itself has an electrolyte and a diaphragm, no further assembly is required and the sample is tested directly on the working electrode and the counter electrode. Cyclic voltammetry (CV) measurements were carried out at speeds ranging from 10 to 100 mV s^{-1}, 100 to 500 mA cm^{-3} and charge and discharge tests were performed at

current densities of 3, 5 and 7 mA cm^{-2}, respectively. The specific capacitance Cs, energy density W and power density P can be calculated from the CV curve as follows:

$$Cs = \frac{\int_{v_1}^{v_2} |I| dv}{Sv\Delta v}$$

$$W = \frac{Cs\Delta v^2}{2}$$

$$P = \frac{W}{\Delta t}$$

Where I is the charging discharge current, S is the area of the entire supercapacitor, $\triangle t$ is the discharge time, V is the scanning rate in the measurement process, and $\triangle V$ is the potential window in CV measurement process.

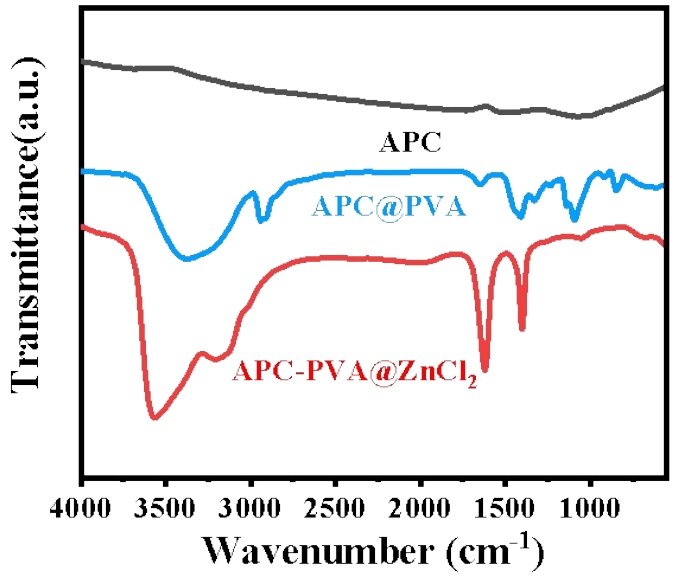

Figure S1 FTIR images of APC, APC@PVA and APC-PVA@$ZnCl_2$.

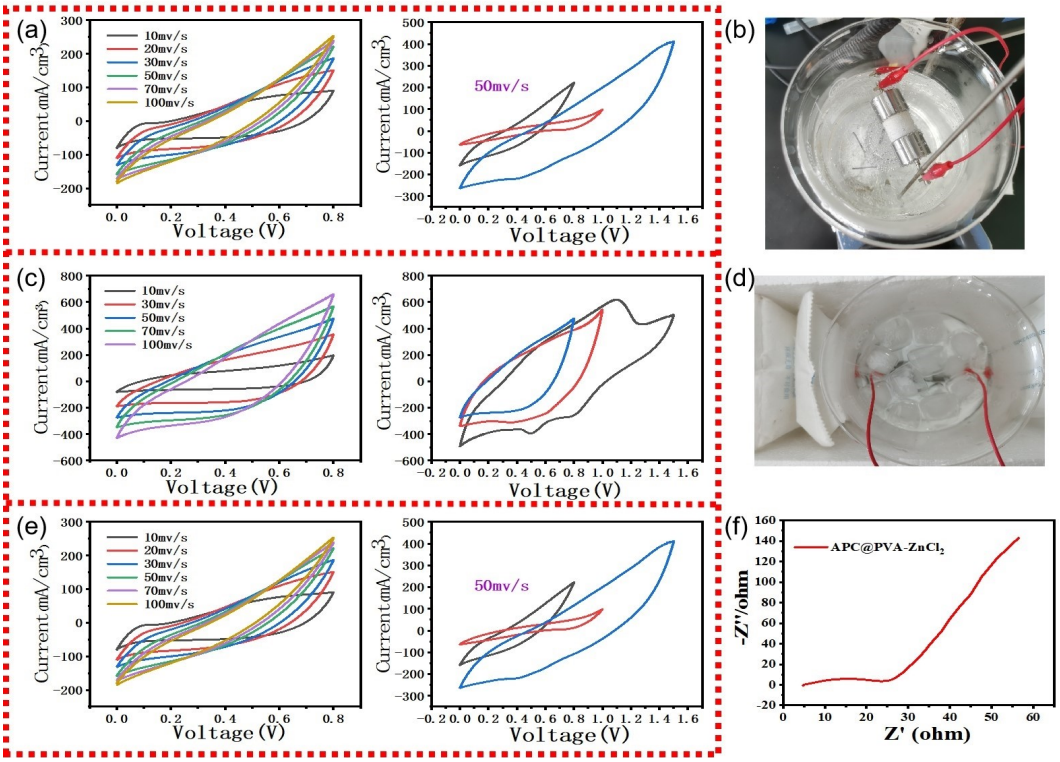

Figure S2 (a) CV curves of the APC-PVA@$ZnCl_2$ and comparison of CV curves of the APC-PVA@$ZnCl_2$ under different potential windows at a scan rate of 50 mVs^{-1} at 25 ℃ , (b) 80 ℃ high temperature environment simulation; (c) CV curves of the APC-PVA@$ZnCl_2$ and comparison of CV curves of the APC-PVA@$ZnCl_2$ under different potential windows at a scan rate of 50 mVs^{-1} at 80 ℃, (d) -5 ℃ low temperature environment simulation; (e) CV curves of the APC-PVA@$ZnCl_2$ and comparison of CV curves of the APC-PVA@$ZnCl_2$ under different potential windows at a scan rate of 50 mVs^{-1} at -5 ℃, (f) the Nyquist diagram of the APC-PVA@$ZnCl_2$ supercapacitor.

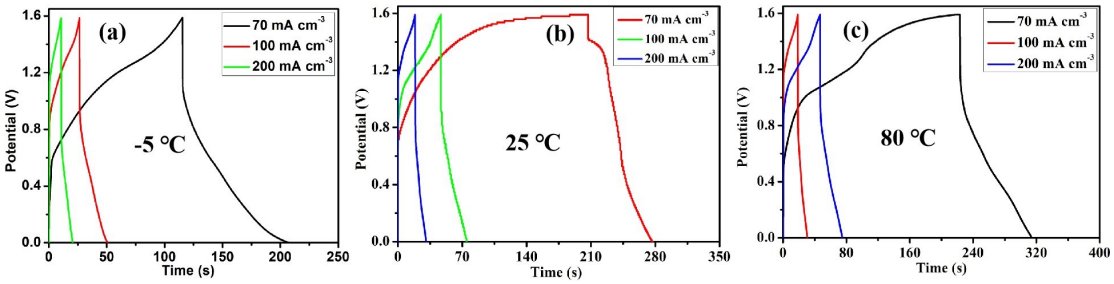

Figure S3 (a) GCD curves of the APC-PVA@$ZnCl_2$ under different current densities and different temperatures under the 0-1.6V potential window. (a) -5 ℃. (b) 25 ℃. (c) 80 ℃.

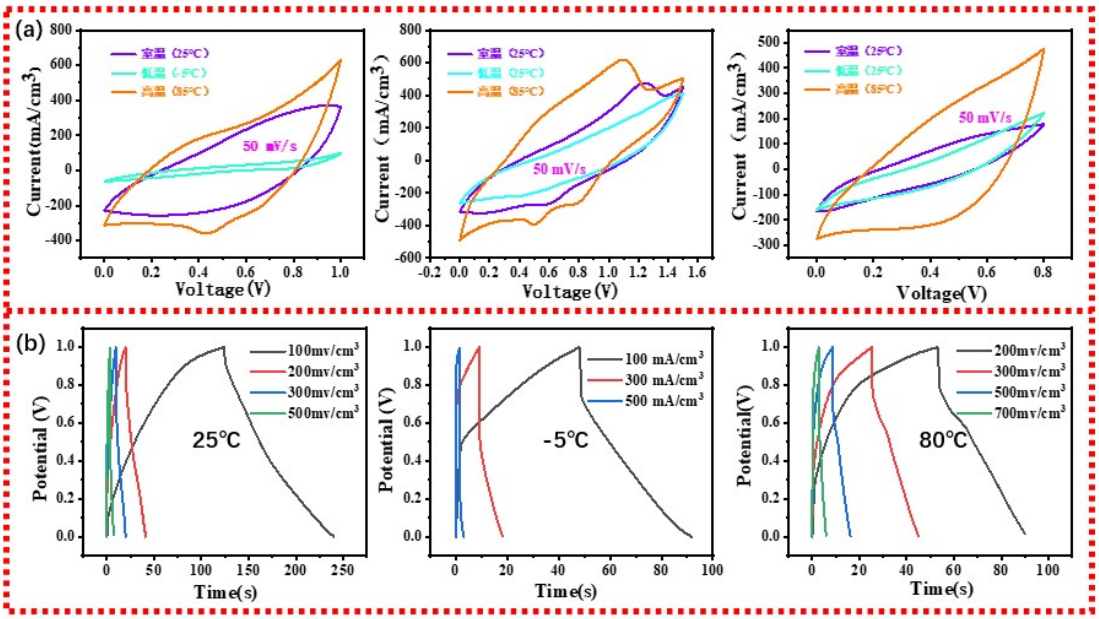

Figure S4 Comparison of CV curves of the APC-PVA@$ZnCl_2$ in different potential windows and ambient temperatures at a scan rate of 50 mV s^{-1}, (b) GCD curves of the APC-PVA@$ZnCl_2$ in different ambient temperatures at various current densities.

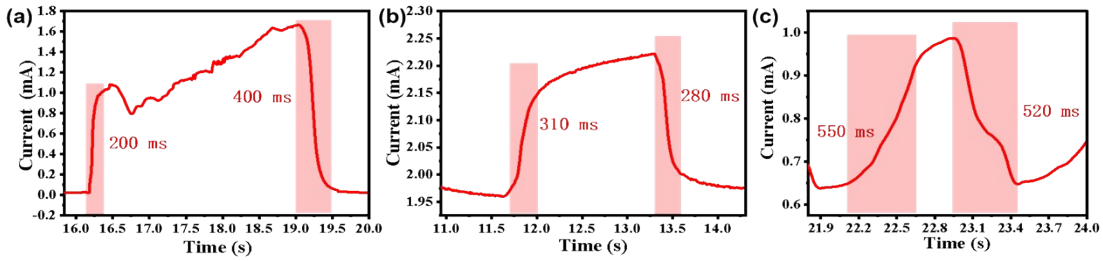

Figure S5 (a) Tension/fracture signal sensitivity, Sensitivity of (b) finger bending and (c) pulse beat sensing signal based on the APC-PVA@$ZnCl_2$ sensor.

Video-1.mp4 Video-2.mp4 Video-3.mp4

Figure S6 The relevant stretching videos of the APC-PVA@$ZnCl_2$.

The device is the home-made ionic Seebeck coefficient measurement setup. The gray region is the measured sample, and the red and blue regions are the heat source and heat sink, respectively, which are powered by the voltage source. The temperature and voltage are recorded by the K-type thermocouple and digitial multimeter, respectively. All the data can be visulized in the computer. The ionic Seebeck coefficient can be obtained by the measured voltage and temperature according to the following equation [1]:

$$S = \frac{V_H - V_C}{T_H - T_C}$$

where the V_H and V_L are the voltage of the heat electrode at temperature T_H and the cold electrode at temperature T_L, respectively.

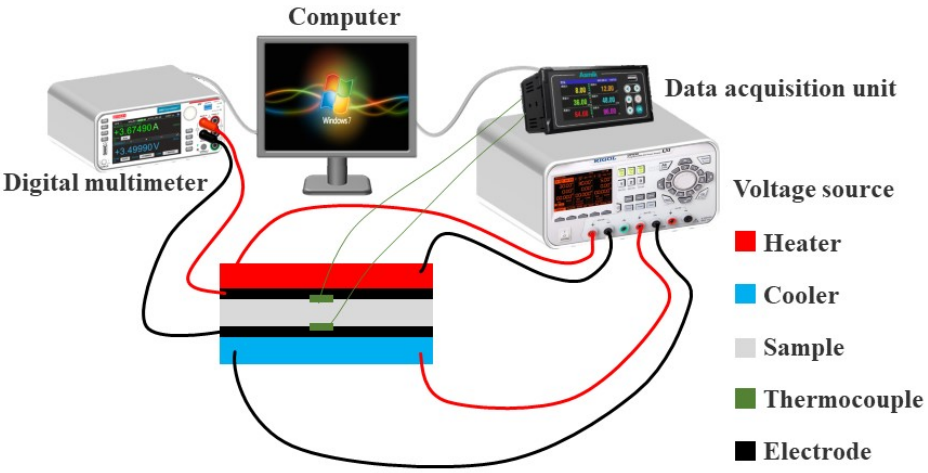

Figure S7 Home-made ionic Seebeck coefficient measurement setup. The red and blue region denote the heat source and heat sink, respectively. The temperature and

voltage are recorded by K-type thermocouple and voltage meter, respectively.

2 Supporting information for molecular dynamics simulations

All molecular dynamics (MD) simulations were performed implemented by the largescale atomic/molecular massively parallel simulator (LAMMPS) package [2]. LigParGen web-based service [3] is used to generate initial structure of APC chain and PVA chain, and obtain the OPLS force-field parameters and partial atomic charges. The TIP4P water model is adopted in our simulations [4]. The non-bonded interactions among ions, water molecules and chains described by Lennard-Jones 12-6 atomistic potential. Initially, the systems with the same mass ratio of synthesis of APC-PVA@$ZnCl_2$ mentioned above are placed in a simulation cell which size depends on maintaining the density of water in the system at 1 g/cm^3 using PACKMOL [5]. Three systems are shown in Figure.1g-i. Periodic boundary conditions in three dimensions were applied. The cut-off radius for long-range energy calculations was set to 12Å. The contribution of long-range interaction was calculated by particle-particle-particle-mesh (PPPM) solver 6]. The Newton's equations of motion were time-integrated with a time-step of 0.1 fs. The Visual Molecular Dynamics (VMD) [7] was used to visualize the trajectories generated during MD simulations. Each sample was equilibrated via the use of NPT simulations at 298 K and 1 atm over a period of 1 ns. Following this, a further 1 ns simulation was performed in the NVT ensemble. Mean square displacement (MSD) can be computed from the following expression,

$$\mathrm{MSD} = \left\langle \frac{1}{N} \sum_{i=1}^{N} \left| r_d - r_d\left(t_0\right) \right|^2 \right\rangle$$

where N is the number of equivalent particles the MSD is calculated over, r is their coordinations and d is the desired dimensionality of MSD. And the radial distribution function (RDF) are calculated by

$$g(r) = \frac{n(r)}{\rho 4\pi r^2 \Delta r}$$

where $n(r)$ is the average number of particles in a spherical shell with a width of Δr at a distance r from the center reference particle, ρ is the average density of particles in the system. The binding energy are calculated by

$$E_{binding} = E_{total} - (E_{chains} + E_{Zn^{2+}})$$

where E_{total} is the energy after stabilization of a system comprising two chains and one Zn^{2+}, E_{chains} and $E_{Zn^{2+}}$ represent the energy after stabilization of tow chains and one Zn^{2+}, respectively. The charge density of each chain was calculated based on the density functional theory using Vienna Ab initio Simulation Package (VASP) [8, 9] along with the projector augmented wave (PAW) pseudopotentials. The Becke-Lee-Yang-Parr (BLYP) version of the generalized gradient approximation (GGA) [10] is used for the exchange-correction function. The convergence criteria for the total energy and ionic force were 1×10^{-8} eV and 0.02 eV·Å^{-1}, respectively. The cutoff energy of the plane-wave was set at 400 eV.

References

[1] C. Chi, M. An, X. Qi, Y. Li, R. Zhang, G. Liu, C. Lin, H. Huang, H. Dang, B. Demir, Nat. Commun. 2022, 13(1), 221.

[2] S. Plimpton S, J. Comput. Phys. 1995, 117(1), 1-19.

[3] LS. Dodda, IC. De Vaca, J. Tirado-Rives J, WL. Jorgensen, Nucleic Acids Res. 2017, 45(W1), W331-W336.

[4] WL. Jorgensen, J. Chandrasekhar, JD. Madura, RW. Impey, ML. Klein, J. Chem. Phys. 1983, 79(2), 926-935.

[5] L. Martínez, R. Andrade, EG. Birgin, JM. Martínez, J. Comput. Chem. 2009, 30(13), 2157-2164.

[6] B. Liao, J. Wang, X. Han, R. Wang, K. Lv, Y. Bai, H. Jiang, Z. Shao, Y. Wang, J. Sun, Chem. Eng. J. 2022, 430, 133098.

[7] W. Humphrey, A. Dalke, K. Schulten K, J. Mol. Graph. 1996, 14(1), 33-38.

[8] G. Kresse, J. Furthmüller, Phys. Rev. B 1996, 54(16), 11169.

[9] G. Kresse G, D. Joubert, Phys. Rev. B 1999, 59(3): 1758.

[10] PM. Gill, BG. Johnson, JA. Pople, Chem. Phys. Lett. 1992, 197(4-5), 499-505.